JOURNAL OF MATERIALS SCIENCE **37** (2002) 4627–4632

Synthesis of zinc oxide/silica composite nanoparticles by flame spray pyrolysis

T. TANI*, L. MÄDLER, S. E. PRATSINIS†
Institute of Process Engineering, ETH Zurich, Sonneggstrasse 3, CH-8092 Zurich, Switzerland
E-mail: pratsinis@ivuk.mavt.ethz.ch

Zinc oxide (ZnO)/silica (SiO_2) composite nanoparticles were made by flame spray pyrolysis. The effects of the Zn/Si ratio on particle properties were examined and compared with those of the pure ZnO and SiO_2 particles made at the same conditions. Polyhedral aggregates of nano-sized primary particles were obtained in all experiments. The mixed-oxide primary particle size was smaller than that of pure oxides. The primary particles consisted of ZnO nano-crystals and amorphous SiO_2, as seen by high-resolution transmission electron microscopy (HR-TEM) and X-ray diffraction (XRD) analysis using the fundamental parameter approach. The XRD size of ZnO was controlled from 1.2 to 11.3 nm by the initial precursor composition and it was consistent with HR-TEM. The composite particles exhibited an excellent thermal stability and little crystalline growth of ZnO (e.g., from 1.9 to 2.2 nm) was observed even after calcination at 600°C.

1. Introduction

Zinc oxide (ZnO) has excellent chemical, electrical and optical properties that find applications as reinforcing filler for elastomer [1], catalyst [2, 3], varistor [4–6], electrode of solar cells [7], photocatalyst [8] and UV-attenuating material [9].

The instability of ZnO nanoparticles is, however, a problem in most specialized applications. For example, sol-gel derived ZnO nanoparticles increased their diameter by aging for a few days, resulting in a significant red shift in the absorption spectra [10]. The specific surface area (SSA) of the ZnO nanoparticles decreased from 130 to 70 m^2/g after calcination at 400°C [11], reducing the number of reactive sites and thus degrading their catalytic performance. To suppress ZnO nanoparticle growth by aging, Mikrajuddin *et al*. [12] made ZnO/SiO_2 composite particles, in which crystalline ZnO particles of ~3 nm in size were dispersed in amorphous SiO_2, by a combination of sol-gel synthesis and spray drying. They observed no change in photoluminescence spectra for over 30 days. However, they focused mainly on the optical properties and therefore the particle SSA and thermal stability were not evaluated to better understand how ZnO was stabilized. Cannas *et al*. [13] also produced ZnO/SiO_2 composite particles, in which amorphous ZnO particles were dispersed in amorphous SiO_2, by the sol-gel method. They evaluated the reaction between ZnO and SiO_2 by the ^{29}Si MAS NMR measurement without presenting the corresponding particle characteristics.

Flame synthesis [14] is one of the established commercial processes to make inexpensive ceramic nanoparticles (SiO_2, TiO_2: less than $5/kg). Especially, flame spray synthesis or pyrolysis (FSP) is a promising technique because a variety of liquid precursors are available for powder synthesis, though FSP is not an established industrial process yet [15, 16]. Synthesis of ZnO [17, 18], $MgAl_2O_4$ [19], β''-alumina [20], TiO_2, CeO_2, CaO, MgO and CeO_2/ZrO_2[21] by FSP have been reported and effects of the oxidant/dispersant flow rate and fuel species on the SSA of SiO_2 powder were systematically examined by Mädler *et al*. [22].

The goal of this study is to synthesize ZnO/SiO_2 nano-composite particles in which crystalline ZnO nanoparticles are dispersed using FSP. Especially, the focus is on the size control and stabilization of ZnO nanoparticles and the effect of precursor Zn/Si ratio on the product particle properties.

2. Experimental

Zinc acrylate (ZA: Fluka, 98%) and hexamethyldisiloxane (HMDSO: Fluka 99%) were used as Zn and Si sources, respectively. A mixture of 94 vol% methanol (J.T. Baker, exceed ACS grade) and 6 vol% acetic acid (Scharlau, reagent grade) was used as solvent. After dissolving ZA in the solvent and adding HMDSO, the liquid was mixed ultrasonically to obtain a transparent solution. The amounts of ZA and HMDSO were varied to obtain particles with the different compositions at Zn molar ratios, $X = 0 - 1$, where X is:

$$X = Zn/(Zn + Si). \quad (1)$$

The concentration of the total metal atoms (Zn + Si) in the precursor solutions was adjusted to be 0.5 mol/L for all experiments.

*On leave from Toyota Central R&D Labs., Inc., Nagakute, Aichi 480-1192, Japan.
†Author to whom all correspondence should be addressed.

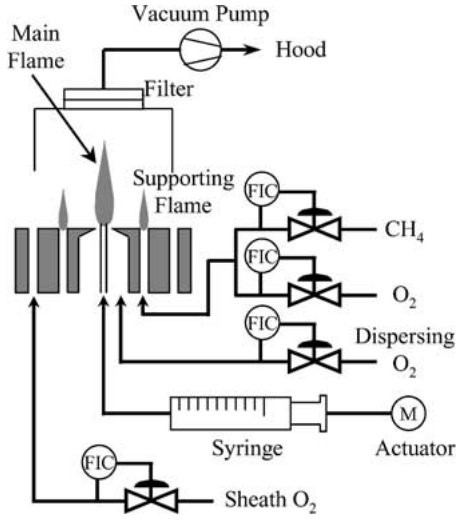

Figure 1 Schematic of the flame spray pyrolysis (FSP) process for synthesis of ZnO/SiO_2 particles.

Powder synthesis was carried out using a spray flame reactor with an oxygen-assisted nozzle [22]. A schematic of the set-up is shown in Fig. 1. The glass syringe supplied through the nozzle 1 mL/min of precursor solution that was dispersed by oxygen flow of 3.85 L/min, giving a powder production rate of 1.80 (pure SiO_2) to 2.44 (pure ZnO) g/h. The nozzle was surrounded by eighteen smaller premixed (methane + oxygen) supporting flames, through which the total flow rate of methane and oxygen were 1.58 and 1.52 L/min, respectively. In addition, 9.8 L/min of oxygen was supplied from another ring surrounding the supporting flames to stabilize the entire process. The product particles were collected on a glass fiber filter (Whatman, GF/A) with the aid of a vacuum pump.

The particle morphology was observed by transmission electron microscopy (TEM: Hitachi, H600, 100 kV) and high-resolution TEM (HR-TEM: Philips, CM30ST, 300 kV). The powder crystallinity was measured by X-ray diffraction (XRD: Bruker, AXS D8 Advance, 40 kV, 40 mA) at $2\theta(\text{Cu } K_\alpha) = 20$–$70^\circ$, step $= 0.02^\circ$ and scan speed $= 0.24^\circ$/min. The crystallite size (d_{CF}) of ZnO was calculated from the XRD patterns using the software (Topas 2.0, Bruker AXS, 2000) based on the fundamental parameter approach [23, 24], in which the effects of the equipment (e.g. X-ray source, slits etc.) were incorporated. The analysis was carried out by fitting the XRD pattern with the crystalline data of zincite [25], assuming that (a) the background was a linear function, (b) the contribution of amorphous SiO_2 was described by a broad peak in the range of $2\theta = 26$–30° and (c) there is no micro-strain in the particles. Only the background level, the position of the amorphous peak, the crystallite size of ZnO and the intensities of the peaks were varied to fit the measured spectra. The ZnO crystallite size (d_{CS}) was calculated also from the full width at half maximum (FWHM) of the (100) peak using Scherrer's equation [26] as it is typically done:

$$d_{CS} = 0.9^*\lambda/(\beta - \beta')\cos\theta, \qquad (2)$$

where λ is a wave length of the X-ray (0.154186 nm) and β, β' and θ represent the measured FWHM, the broadening of the peak caused by the equipment and a diffraction angle, respectively. The β' was determined to be 0.141° by measuring the FWHM of the (100) peak using the ZnO particles of several microns in diameter.

The specific surface area (SSA) of the particles was measured by 5-point nitrogen adsorption (BET: Micromeritics, Gemini 2350) after degassing the powder at 150°C for 2 hours in nitrogen. The equivalent average primary particle diameter (d_{BET}) was calculated from the measured SSA and the density (ρ) of the particles using: $d_{BET} = 6/(\text{SSA}^*\rho)$, assuming that ρ is given by:

$$\rho = X^*\rho_{ZnO}(5.61 \times 10^3\ \text{kg/m}^3) + (1 - X)^*\rho_{SiO_2}(2.2 \times 10^3\ \text{kg/m}^3). \qquad (3)$$

The product powder was calcined in an alumina crucible at 600°C for 2 hours in air (Carbolite, CWF 13/23) to evaluate the thermal stability of ZnO particles.

3. Results

Fig. 2 shows TEM micrographs of pure ZnO ($X = 1$), 2 : 1 $ZnO : SiO_2$ mixture ($X = 0.67$) and pure SiO_2 ($X = 0$) made by FSP. All powders were polyhedral aggregates of primary particles with average diameters of 10, 8 and 20 nm for $X = 1$, 0.67 and 0, respectively. The growth of the primary particles was suppressed clearly when mixed oxides were produced.

Fig. 3 shows a HR-TEM micrograph of $X = 0.67$. Each primary particle was a nano-composite, in which very fine crystals of 1–3 nm in diameter were dispersed in the amorphous phase. The observed lattice distance (Fig. 3) was 0.163 nm, which was in agreement with the distance (0.162 nm) of the (110) plane in hexagonal ZnO (zincite, #36-1451).

Fig. 4 shows XRD patterns of the FSP-made particles. The pure ZnO particles ($X = 1$) were zincite (#36-1451). The diffraction peaks were observed at the same angles as those of the pure ZnO particles in the mixed system, although the peaks were diffused with increasing SiO_2 concentration. No zinc silicates (e.g. willemite) were observed in any powders. Fig. 5 shows how the fundamental parameter approach of the XRD pattern is used to determine the phase composition for $X = 0.67$ as a typical example. The XRD pattern was described well as the sum of the linear background, the crystalline ZnO and the broad peak attributed to an amorphous phase (e.g. SiO_2).

Fig. 6 shows crystallite sizes (d_{CF} or d_{CS}) of ZnO and BET-equivalent average primary particle diameter (d_{BET}) for various Zn/Si ratios. It was difficult, however, to determine the d_{CF} (fundamental parameter approach) in the range of $X < 0.4$ because the peaks were too weak to be determined. It was also difficult to measure the FWHM for the calculation of the d_{CS} (Scherrer's equation) in the range of $X < 0.9$ because of an overlapping of the diffraction peaks. The d_{CF} and d_{CS} were in good agreement with each other for both $X = 1$ and 0.9, although the accuracy of d_{CS} in $X = 0.9$ is questionable because it is difficult to determine FWHM in crystals of less than 4 nm even in a simple system [27] and the amorphous phase can affect the shape of the ZnO peaks here. The d_{CF} of the pure ZnO particles ($X = 1$)

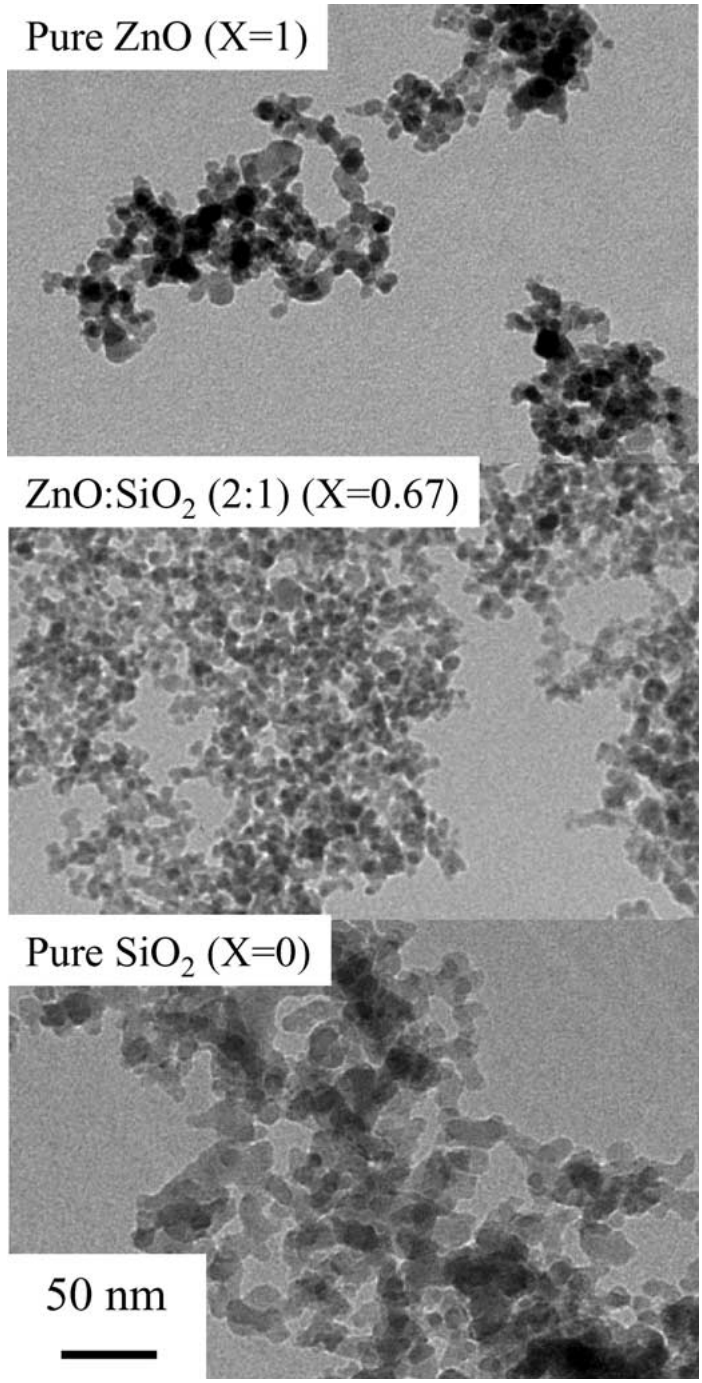

Figure 2 Transmission electron microscopic images of FSP-made powders of pure ZnO ($X = 1$), 2 : 1 $ZnO : SiO_2$ mixture ($X = 0.67$) and pure SiO_2 ($X = 0$). Mixed oxide particles appear to be smaller than either oxide made alone.

was in agreement with the TEM primary particle sizes, indicating that the primary particles were single crystallites. In the mixed oxides, the d_{CF} of ZnO decreased from 3.9 (at $X = 0.9$) to 1.2 nm (at $X = 0.4$) as the content of Si increased. At $X = 0.67$, the $d_{CF} = 2.2$ nm was also in agreement with the observed crystallite size in the HR-TEM micrograph (Fig. 3).

In the mixed oxides, the d_{BET} was smaller than those of pure ZnO and SiO_2 and decreased from 8.6 (at $X = 0.9$) to 5.0 nm (at $X = 0.2$) as the content of Si increased. Especially, the remarkable decrease of d_{BET} (by factor of 3.7) was observed by substituting 20 mol% of Si with Zn. The d_{BET} of $X = 1$, 0.67 and 0 were consistent with the TEM primary particle sizes (Fig. 2). The d_{BET} of $X = 1$ was also in good agreement with the XRD crystallite size. The d_{BET} were larger by factor of 2–4 than d_{CF} in the composite system, showing that the primary particles were not ZnO single crystals but the composite as seen in Fig. 3.

Fig. 7 shows intensities of the ZnO and amorphous phases in the calculated XRD patterns, which corresponds most likely to the amount of each phase. The intensities of the ZnO and amorphous phases increased and decreased, respectively, as the amount of Si decreased, suggesting that the amorphous phase in the composite system corresponds to amorphous SiO_2.

Fig. 8 shows XRD patterns of powders made at $X = 1$, 0.8, 0.67 and 0.4 before (dashed lines) and after (solid lines) the calcination at 600°C for 2 hours. The XRD peaks obviously became sharper in the calcined

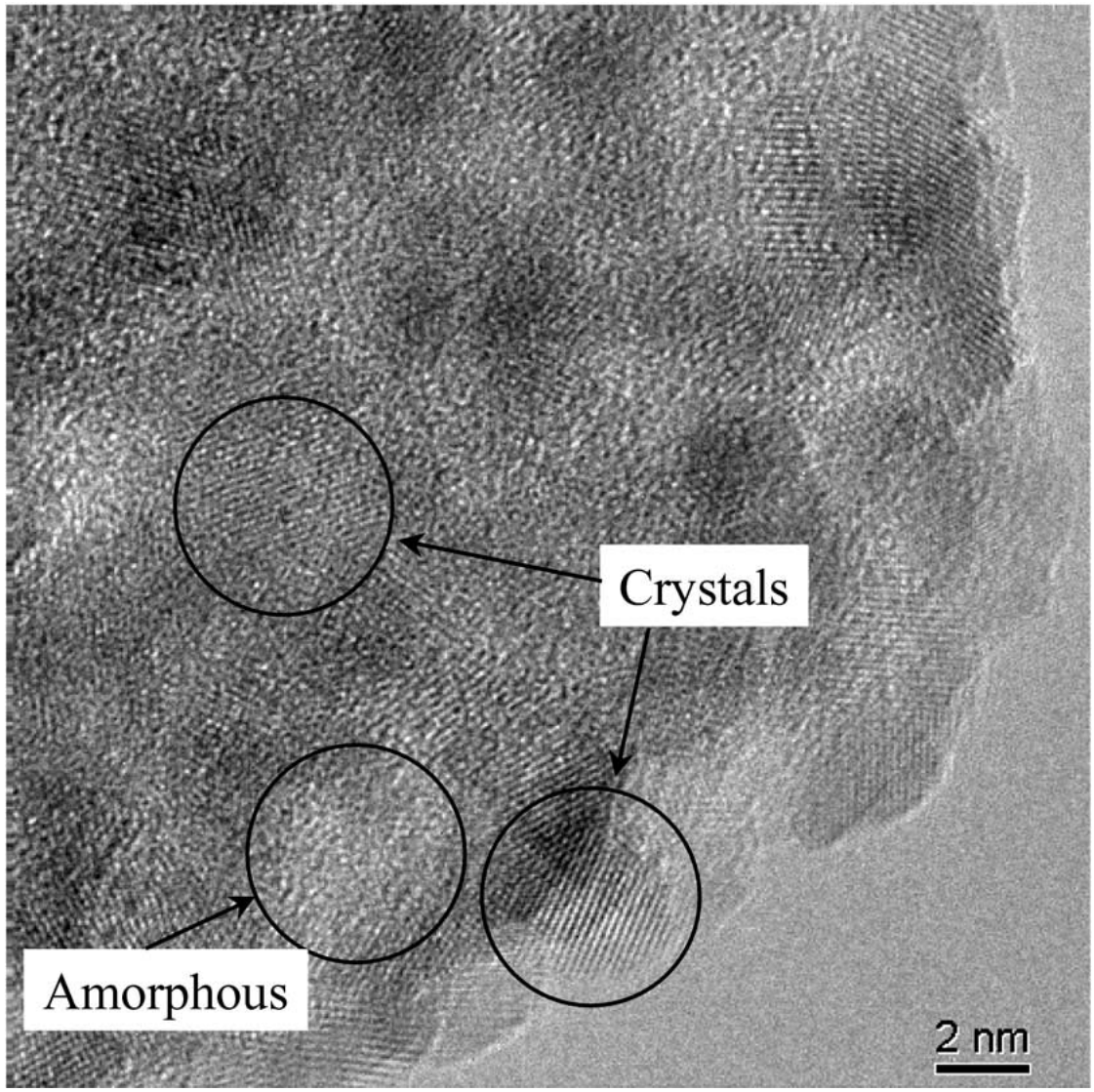

Figure 3 High-resolution transmission electron microscopic image of ZnO/SiO_2 powder with $X = 0.67$.

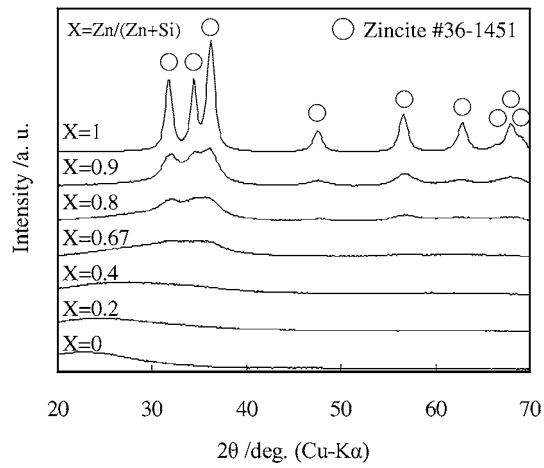

Figure 4 X-ray diffraction patterns of ZnO/SiO_2 powder with $X = 1$, 0.9, 0.8, 0.67, 0.4, 0.2 and 0.

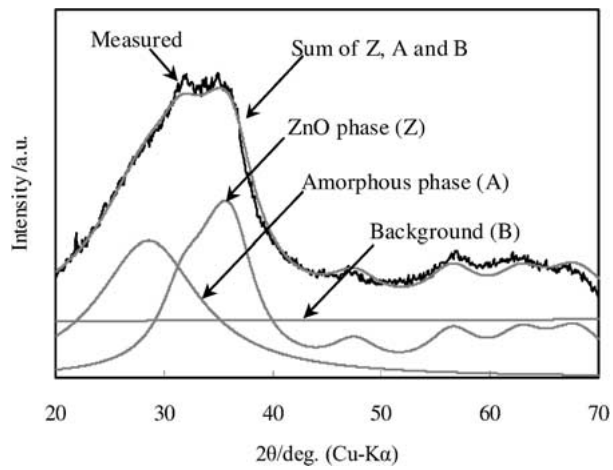

Figure 5 Result of the fitting using the fundamental parameter approach in ZnO/SiO_2 powder with $X = 0.67$. The black and gray lines correspond to the measured and calculated XRD patterns, respectively.

pure ZnO ($X = 1$) compared with that before calcination, resulting in the increase of the d_{CS} from 10.7 to 25.6 nm. On the contrary, the XRD patterns were hardly changed by calcination of the mixed system, which indicates that only little crystalline growth of ZnO (e.g. from 1.9 to 2.2 nm) occurred till 600°C, confirming the stabilization role of SiO_2.

4. Discussion

Polyhedral aggregates are observed typically with vapor flame-made SiO_2 and TiO_2 [14]. Because of the similarity in particle morphology of vapor flame and spray flame-made particles, it can be inferred that particles here were formed in the gas phase. In the mixed

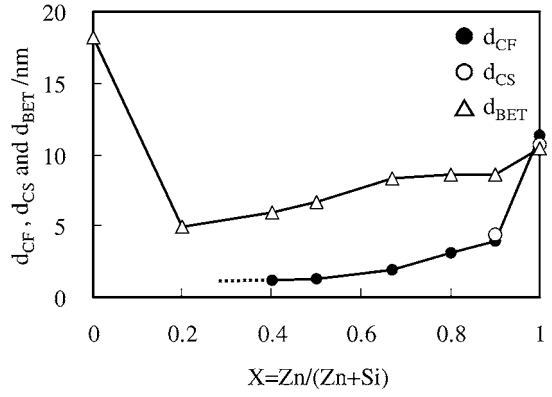

Figure 6 Crystallite sizes of ZnO and BET equivalent mixed or pure oxide average primary particle diameter as function of Zn/Si ratio. Solid and open circles correspond to the crystallite sizes calculated using the fundamental parameter approach (d_{CF}) and Scherrer's equation (d_{CS}), respectively. Open triangles represent the BET equivalent average primary particle diameter (d_{BET}).

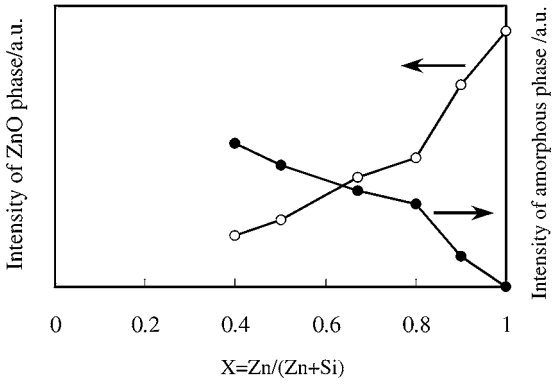

Figure 7 Intensities of the ZnO and the amorphous phase in the calculated XRD patterns.

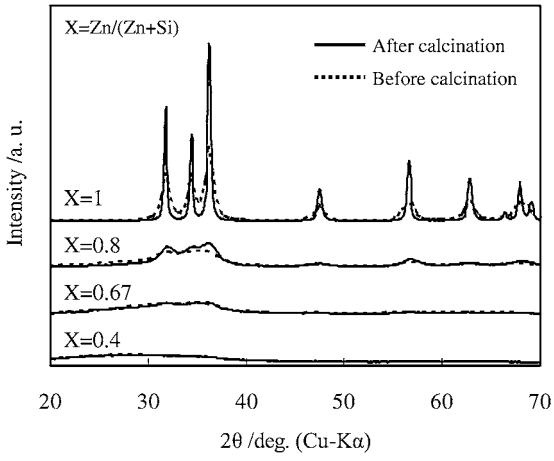

Figure 8 XRD patterns of ZnO/SiO_2 powder with $X = 1$, 0.8, 0.67 and 0.4 before (dashed lines) and after (solid lines) the calcination at 600°C.

system, ZnO nanoparticles were dispersed in amorphous SiO_2, judging from the HR-TEM and XRD results.

Vemury and Pratsinis [28] investigated the effects of dopants on the particle properties of TiO_2 in flame aerosol synthesis. They reported that the SSA increased by the doping of Si because (a) the sintering rate of TiO_2 was much faster than that of SiO_2, (b) TiO_2 were formed first and SiO_2 followed and (c) the presence of SiO_2 suppressed the sintering of TiO_2. They also reported that the SSA decreased by the doping of Sn and Al except for the 5 mol% of Sn doping (the lowest amount of the doping in their experiments) by the substitution of Sn^{4+} and Al^{3+} to Ti^{4+} site because of the similarity of the ionic radius, enhancing the sintering. Jensen et al. [29] reported ZnO-Al_2O_3 particle synthesis by flame aerosol synthesis, in which $ZnO/ZnAl_2O_4$ mixed powder was obtained when substituting 15 or 36 mol% of Zn with Al. The d_{BET} in the mixed system decreased by factor of 3 compared with pure ZnO. The particle growth suppression was observed when Zn reacts with Al to form $ZnAl_2O_4$ which is different from ZnO/SiO_2 mixture. Although Jensen *et al*. [29] did not propose a detailed mechanism of the particle growth suppression, they considered that $ZnAl_2O_4$ was formed first followed by nucleation of excess ZnO. In their case, the particle growth suppression was attributed to the presence of two different particles or nuclei in the flame as it was reported in former studies [28]. In this study, Zn^{2+} and Si^{4+} cannot be substituted with each other, because the ionic radius of Zn^{2+} (0.60 Å) is quite different from that of Si^{4+} (0.26 Å) [30]. Furthermore, the formation of Zn_2SiO_4 (willemite) may be difficult at residence times in the order of milliseconds in the spray flame as post-calcination at 1000°C was necessary to obtain willemite from the spray pyrolysis-made particles [31, 32], although Lenggoro *et al*. [33] directly synthesized willemite by spray pyrolysis allowing for long residence time (4 sec.) in the hot zone. Therefore, it can be concluded that the ZnO and SiO_2 clusters coexist without substitution or reaction hindering each other's grain growth.

Molten SiO_2 clusters may be formed first here, judging from the fact that the boiling point of SiO_2 (2950°C) [30] is higher than the sublimation point of ZnO (∼2000°C) [34]. The melting point of SiO_2 is 1713°C [30], which means that the solidification of molten SiO_2 occurs after nucleation of the solid ZnO. Although these data refer to the bulk oxides that can be different from those of nanoparticles, the order of the phenomena during cooling is considered to be same between them in the nanoscale. Therefore, the composite particle could be formed by condensation of SiO_2 clusters from the gas phase followed by formation of solid ZnO clusters from the gas phase on the molten SiO_2 followed by subsequent solidification to form the primary composite particle after smoothing the surface of the particle by surface tension as observed by TEM (Fig. 2). These considerations are in agreement with the discussion of Vemury and Pratsinis [28] for the TiO_2/SiO_2 system.

The increase of Zn concentration in the precursor can enhance the coagulation and/or the surface growth of the ZnO clusters on the molten SiO_2, increasing the d_C (Fig. 6). The agreement of the TEM diameter (Fig. 2) and d_{BET} (Fig. 6) in the mixed system can be explained by the formation of the smooth spherical particles. The pure SiO_2 ($X = 0$) primary particles were larger than pure ZnO ($X = 1$) made at the same conditions, suggesting that the sintering rate of SiO_2 is faster than that of ZnO. This can indicate that suppression of particle

growth by the presence of the other oxide is more effective for pure SiO_2 rather than ZnO, resulting in the significant decrease of d_{BET} when substituting Si with Zn.

On the other hand, Vemury and Pratsinis [28] also reported that the doping of Si in TiO_2 inhibited phase transformation from anatase to rutile because the ionic radius of Si^{4+} was small enough to enter the titania lattice interstitially, locking the lattice to inhibit phase transformation. Here, some of Si^{4+} ions can enter the zinc oxide lattice interstitially at the surface because of the large difference of the ionic radius between Zn^{2+} and Si^{4+}, which may suppress the crystalline growth of ZnO.

The ZnO nanoparticles seem to exist independently and to be surrounded by amorphous SiO_2. In this condition, the solid-state diffusion of the metal ions can be suppressed because Zn^{2+} and Si^{4+} cannot be substituted with each other and the calcination temperature of 600°C is too low to form willemite, judging from the fact that β-willemite was crystallized at 722°C from sol-gel derived amorphous Zn_2SiO_4 [35]. Therefore a high thermal stability of the ZnO nanoparticles was achieved in the mixed system. From these properties, these composite particles can be quite attractive for catalysts [11] and optical materials [10].

5. Conclusions

ZnO/SiO_2 composite nanoparticles were made by FSP. Polyhedral aggregates of nano-sized primary particles were obtained in all experiments. The primary particles consisted of ZnO nano-crystals and amorphous SiO_2. The XRD crystallite size of ZnO, d_{CF}, was analyzed using the fundamental parameter approach and controlled from 1.2 (at $X = 0.4$) to 11.3 nm (at $X = 1$) by changing the composition of the precursor. The BET equivalent average primary particle diameter (d_{BET}) decreased by the mixing of Zn and Si. The d_{BET} decreased from 10.4 (at $X = 1$) to 5.0 nm (at $X = 0.2$) and then increased to 18.2 nm (at $X = 0$). In the mixed system, the d_{BET} was larger by factor of 2–4 than the d_{CF}. The composite particles exhibited an excellent thermal stability and little crystalline growth of ZnO was observed after calcination at 600°C for 2 hours, e.g. from 1.9 to 2.2 nm.

Acknowledgement

The authors are grateful to Dr. Frank Krumeich (ETHZ) and Dr. Martin Müller (ETHZ) for the HR-TEM observation and providing the TEM equipment, respectively. This research was funded by Toyota Central R&D Labs., Inc. and Kommission für Technologie und Innovation (KTI) TOP NANO 21, grant #5351.1, Switzerland.

References

1. R. C. KLINGENDER, M. OYAMA and Y. SAITO, *Rubber World* **202** (1990) 26.
2. D. S. KING and R. M. NIX, *J. Catal.* **160** (1996) 76.
3. M. CONSONNI, D. JOKIC, D. Y. MURZIN and R. TOUROUDE, *ibid.* **188** (1999) 165.
4. S. HINGORANI, V. PILLAI, P. KUMAR, M. S. MULTANI and D. O. SHAH, *Mater. Res. Bull.* **28** (1993) 1303.
5. M. SINGHAL, V. CHHABRA, P. KANG and D. O. SHAH, *ibid.* **32** (1997) 239.
6. S. BOILY, H. ALAMDARI, G. CROSS, A. JOLY, A. VANNESTE, P. GRUTTER and R. SCHULZ, in "Synthesis and Properties of Mechanically Alloyed and Nanocrystalline Materials, Pts. 1 and 2—Ismanam-96" (Transtec Publications Ltd, Zurich-Uetikon, 1997) p. 993.
7. H. RENSMO, K. KEIS, H. LINDSTROM, S. SODERGREN, A. SOLBRAND, A. HAGFELDT, S. E. LINDQUIST, L. N. WANG and M. MUHAMMED, *J. Phys. Chem.* B **101** (1997) 2598.
8. K. Y. JUNG, Y. C. KANG and S. B. PARK, *J. Mater. Sci. Lett.* **16** (1997) 1848.
9. T. IWASAKI, M. SATOH, T. MASUDA and T. FUJITA, *J. Mater. Sci.* **35** (2000) 4025.
10. S. MONTICONE, R. TUFEU and A. V. KANAEV, *J. Phys. Chem.* B **102** (1998) 2854.
11. C. L. CARNES and K. J. KLABUNDE, *Langmuir* **16** (2000) 3764.
12. MIKRAJUDDIN, F. ISKANDAR, K. OKUYAMA and F. G. SHI, *J. Appl. Phys.* **89** (2001) 6431.
13. C. CANNAS, M. CASU, A. LAI, A. MUSINU and G. PICCALUGA, *J. Mater. Chem.* **9** (1999) 1765.
14. S. E. PRATSINIS, *Prog. Energy Combust. Sci.* **24** (1998) 197.
15. M. SOKOLOWSKI, A. SOKOLOWSKA, A. MICHALSKI and B. GOKIELI, *J. Aerosol Sci.* **8** (1977) 219.
16. H. K. KAMMLER, L. MÄDLER and S. E. PRATSINIS, *Chem. Eng. Technol.* **24** (2001) 583.
17. J. W. CARROZ, F. K. ODENCRANTZ, W. G. FINNEGAN and D. C. DREHMEL, *Am. Ind. Hyg. Assoc. J.* **41** (1980) 77.
18. T. TANI, L. MÄDLER and S. E. PRATSINIS, *J. Nanoparticle Res.*, in press.
19. C. R. BICKMORE, K. F. WALDNER, D. R. TREADWELL and R. M. LAINE, *J. Amer. Ceram. Soc.* **79** (1996) 1419.
20. A. C. SUTORIK, S. S. NEO, D. R. TREADWELL and R. M. LAINE, *ibid.* **81** (1998) 1477.
21. R. M. LAINE, T. HINKLIN, G. WILLIAMS and S. C. RAND, in "Metastable, Mechanically Alloyed and Nanocrystalline Materials," Pts. 1 and 2 (Trans Tech Publications Ltd, Zurich-Uetikon, 2000) p. 500.
22. L. MÄDLER, H. K. KAMMLER, R. MUELLER and S. E. PRATSINIS, *J. Aerosol Sci.* **33** (2002) 369.
23. R. W. CHEARY and A. COELHO, *J. Appl. Crystallogr.* **25** (1992) 109.
24. *Idem., ibid.* **31** (1998) 862.
25. J. ALBERTSSON, S. C. ABRAHAMS and A. KVICK, *Acta Crystallogr. Sect. B-Struct. Commun.* **45** (1989) 34.
26. R. C. RAU, *Advance in X-Ray Analysis* **5** (1962) 104.
27. W. GERHARTZ, in "Ullmanns Encyklopadie der technischen Chemie" (Verlag Chemie, Weinheim, 1972) Band 5, p. 256.
28. S. VEMURY and S. E. PRATSINIS, *J. Amer. Ceram. Soc.* **78** (1995) 2984.
29. J. R. JENSEN, T. JOHANNESSEN, S. WEDEL and H. LIVBJERG, *J. Nanoparticle Res.* **2** (2000) 363.
30. D. R. LIDE, in "CRC Handbook of Chemistry and Physics," 81st ed. (CRC Press, Boca Raton, 2000) p. 4–85 and 12–15.
31. R. MORIMO, R. MOCHINAGA and K. NAKAMURA, *Mater. Res. Bull.* **29** (1994) 751.
32. Y. C. KANG and S. B. PARK, *ibid.* **35** (2000) 1143.
33. I. W. LENGGORO, F. ISKANDAR, H. MIZUSHIMA, B. XIA, K. OKUYAMA and N. KIJIMA, *Jpn. J. Appl. Phys. Part 2—Lett.* **39** (2000) L1051.
34. M. SUZUKI, M. KAGAWA, Y. SYONO and T. HIRAI, *J. Mater. Sci.* **27** (1992) 679.
35. C. C. LIN and P. Y. SHEN, *J. Solid State Chem.* **112** (1994) 387.

Received 23 October 2001
and accepted 18 July 2002